NATIONAL ENERGY TECHNOLOGY LABORATORY

OIL & GAS

DOE Award No.: DE-FE00-28966

Final Project Scientific / Technical Report

Impact of clays on the compressibility and permeability of sands during methane extraction from gas hydrate

Project Period (10/1/2016 to 6/30/2019)

Submitted by:
Dr. Jongwon Jung

Signature

Louisiana State University, Dept. of Civil and Environmental Engineering
DUNS #075050765
3505C Patrick Taylor Hall
Baton Rouge, LA 70803
Email: jjung@lsu.edu
Phone number: (225) 578-9471

Prepared for:
United States Department of Energy
National Energy Technology Laboratory

July 25, 2019

U.S. DEPARTMENT OF ENERGY | NATIONAL ENERGY TECHNOLOGY LABORATORY

Office of Fossil Energy

DISCLAIMER

TABLE OF CONTENTS

EXECUTIVE SUMMARY

Background: The quantity of methane potentially recoverable from gas hydrate is large enough to motivate federally-supported production tests in several countries, which in turn motivates studies of reservoir production efficiency. Evaluating long-term production well viability involves modeling permeability evolution in the reservoir sediments around the production well because processes reducing the flow of gas into the production well also reduce the long-term economic viability of the well. Fine particles, such as clays, exist nearly ubiquitously in the permafrost and marine settings that typically host gas hydrate, and fines reacting to fluid flow by migrating and clogging pore throats can reduce flow toward the production well. Many fines are sensitive to variations in pore-fluid chemistry, swelling in reaction to in situ pore brine being displaced by fresh water liberated from hydrates during dissociation. Additionally, fine particles tend to collect at gas/water interfaces created by the multiphase flow of gas and water. Thus, as methane and fresh water flow from the hydrate-dissociation front toward the production well, fine particles in the reservoir sands, interbedded fine-grained layers and seal layers can be swelled, migrated (or both), potentially clogging pathways and limiting flow to the production well.

Objective: This project provides a quantitative basis for reservoir models to account for the impact of clays and other fine-grained material ("fines") on reservoir compressibility and permeability, two key factors controlling the flow of gas and fluids toward a production well. This overall objective is addressed through a combination of site-specific and more generalized, fundamental science goals:

Site-specific measurement goals: quantify the change in compressibility and permeability due to the reaction of fines to pore-water freshening in sediment collected during gas hydrates research expeditions (2010 UBGH2 expedition offshore eastern Korea; 2015 NGHP-02 expedition offshore eastern India).

Fundamental measurements on pure fines goal: distinguish between, and quantify, mechanisms for sediment compressibility and permeability change due to physical and chemical responses of fines to the flow of freshened pore water and gas:

- Chemical response: quantify and catalog the sensitivity of pure fines (fines with only a single component, or "endmember" fines) to pore-water chemistry.
- Physical response: quantify the link between fines migration and clogging during single and multiphase flow.

Project Description

The overall project is divided into three laboratory Tasks:

Task 1: *Electrical sensitivity of fines*. This Task establishes the extent to which behaviors of specific types of fines change in response to pore-water chemistry changes (such as pore-water freshening during production from gas hydrates).

Task 2: *Fines migration and clogging due to single- and multiphase-fluid flow in 2D microfluidic models*. This Task establishes the extent to which the pure fines from Task 1, as well as site-specific sediment from gas hydrate occurrences offshore India and Korea, migrate through and clog the pore throats of 2D micromodels. As with Task 1, Task 2 looks at how these migration and clogging behaviors change in response to pore-water chemistry changes.

Task 3: *Site-specific analysis: fines impact on compressibility and permeability*. This Task utilizes site-specific sediment from gas hydrate occurrences offshore India to quantify how in situ fines alter sediment compressibility and permeability in response to the flow of freshened water through the sediment.

This report summarizes the original hypotheses and the key results for each Task in this study.

Task 1: Electrical sensitivity of fines

Background and Hypothesis: Previous work demonstrated that fines behave differently when exposed to different fluids. A major premise of this project is that one should be able to estimate the extent of those behavioral changes for a particular site if the mineralogy at that site is known. Making the link between in situ fines and their overall behavior requires an understanding of how each individual fine type responds to pore water chemistry changes, so this project includes an analysis of the fines most commonly occurring in sediments associated with gas hydrate reservoirs. This project task establishes the link between the type of fines and the expected behavioral dependence on pore-water chemistry via three subtasks:

Subtask 1.1: Index properties of pure, endmember fines

Index properties (grain size, grain density, mineralogy and specific surface) were measured on seven commercially-available endmember fines associated with gas hydrate reservoirs: calcium carbonate, diatoms, illite, kaolin, mica, montmorillonite (or bentonite), and silica silt.

Subtask 1.2: Electrical sensitivity of pure, endmember fines

The pure, endmember fines tested in Task 1.1 were measured for electrical sensitivity, which is based on the liquid limits measured in three specific pore fluids: deionized water, NaCl brine, and kerosene. The liquid limit tests will be run using a fall-cone penetrometer and with the three different pore fluids: deionized water, NaCl brine (2M), and kerosene. How electrically sensitive a particular type of fine is indicates how much of a behavioral difference could be expected for that fine if the pore fluid chemistry changes.

Subtask 1.3: Dependence of compressibility on pore-fluid chemistry in pure, endmember fines

The pure, endmember fines tested in Task 1.1 were measured for compressibility in a standard oedometer. For each fine type, the oedometer test was run using deionized water, NaCl brine (2M), and kerosene.

Results and Implications: The results summarized here are now published with additional detail in the *Journal of Geophysical Research* paper by Jang et al. (2018).

Subtask 1.1: Index properties of pure, endmember fines

Index property results are given in Table 1. An important aspect of these results is that certain fines have particular properties that are far from the average results in Table 1. An example would be the grain density of diatoms or the specific surface of bentonite. These outlier properties can help indicate when these fines are present, which is particularly important because diatoms and bentonite can be difficult to identify in X-Ray Diffraction analyses of mineralogy.

Table 1. Index properties of pure fines

Number (Refer to Figure 1)	sediment	specific gravity *Gs*	median particle size D_{50} [μm]	specific surface S_s [m^2/g]
1	silica silt	2.65	10.5	0.2
2	mica	2.82	17	4.2
3	$CaCO_3$	2.73	8	0.2
4	diatoms	2.23	10	98
5	kaolin	2.68	4	24
6	illite	2.71	20	29
7	bentonite	2.53	< 2	579

Subtask 1.2: Electrical sensitivity of pure, endmember fines

Electrical sensitivity classifications are based on the liquid limits evaluated using specific pore-fluid chemistries. In addition to aiding in the electrical sensitivity characterization, liquid limits are themselves useful through their relationships to other physical properties such as hydraulic conductivity

and compressibility of remolded soils. The measured liquid limit and electrical sensitivity classifications are given in Table 2, along with the plastic limits for completeness. The electrical sensitivity classification is shown graphically in Figure 1, indicating that bentonite and kaolin are the most electrically sensitive fines, and should manifest the largest behavioral changes as the pore fluid chemistry changes.

Table 2. Liquid limit (*LL*), plastic limit (PL) and electrical sensitivity classification for pure fine-grained sediments. The limits are measured in deionized water (*DW*), 2M brine (*brine*) and kerosene (*ker*). The electrical sensitivity classification is indicated by two letters: the first describes either no (N), low (L) intermediate (I) or high (H) plasticity fine grains, and the second letter refers to low (L), intermediate (I) or high (H) electrical sensitivity as shown in Figure 1.

Number (Refer to Figure 1)	sediment	liquid limit LL_{DW}	liquid limit LL_{brine}	liquid limit LL_{ker}	plastic limit PL_{DW}	plasticity index $PI=LL-PL$	electrical sensitivity soil classification
1	silica silt	31	31	36	30	1	LI
2	mica	94	81	110	80	14	HI
3	$CaCO_3$	25	23	31	17	8	NI
4	diatoms	119	111	140	98	21	HI
5	kaolin	77	55	83	38	39	II
6	illite	56	52	59	32	24	IL
7	bentonite	288	126	65	54	234	HH

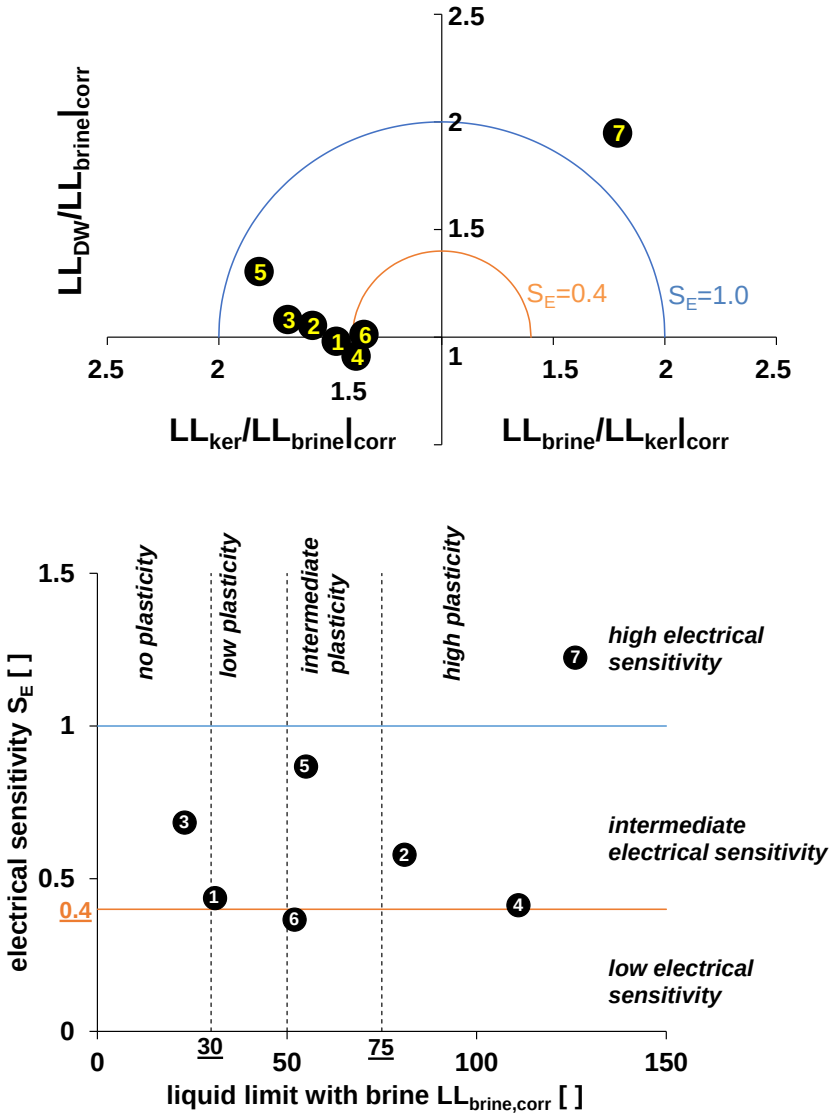

(b)

Figure 1. Charts for soil classification based on electrical sensitivity. Numbered black circles refer to the sediments in Tables 1 and 2. (a) Normalized liquid limit ratio of deionized water and kerosene to brine. The subscript *corr* refers to a correction for the salt mass in the brine and also for the low specific gravity of the kerosene (See Jang et al., 2018, *Journal of Geophysical Research*). (b) Fines classification based on electrical sensitivity, S_E. See Jang et al., 2018, *Journal of Geophysical Research* for details on the corrections and S_E calculations.

Subtask 1.3: Dependence of compressibility on pore-fluid chemistry in pure, endmember fines

Though the electrical sensitivity tests run in Subtask 1.2 are critical for establishing the magnitude of any expected behavior changes for fines

as the pore fluid changes, the tests do not directly indicate the manner in which the fines behavior will change. As pore water freshens during gas hydrate dissociation, for instance, the electrical sensitivity alone will not reveal whether a particular fines behavior will be enhanced or limited. To better understand the compressibility results, it was necessary to examine how pore fluid changes impact the fabric of fines, meaning the manner in which fines cluster and arrange themselves. Figure 2 illustrates the differing ways in which fines can interact electrically based on pore fluid salinity, and these published discussions formed the basis of the hypothesis used in this study.

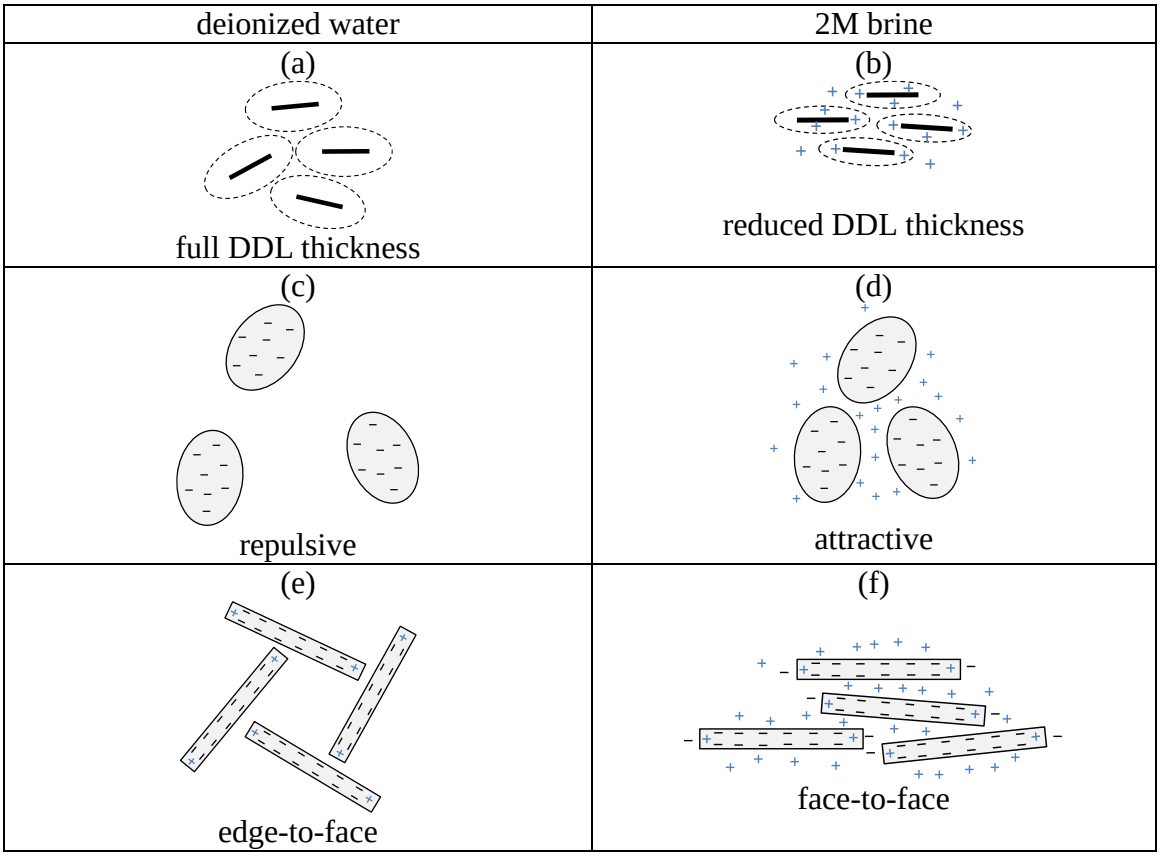

Figure 2. Mechanisms of electrical interactions among particles: (a) fully developed diffusive double layer, DDL, in deionized water and (b) reduced DDL in brine: solid lines are particles and dashed ellipsoids are imaginary DDLs. The Sogami-Ise model shows repulsive and attractive forces due to surface charge interactions between (c) like-charged particles and (d) between particles and ions in surrounding fluid (McBride and Baveye, 2002; Sogami and Ise, 1984). Attractive interactions due to localized surface charge: (e) edge-to-face fabric and (f) face-to-face fabric for larger, platy fines such as kaolin. Face-to-face is more dense, but the clustering occurs more slowly than the edge-to-face arrangement.

A series of sedimentation tests was developed to illustrate how fines cluster in different pore fluids. The sedimentation test schematic is given in Figure 3. As shown in Figure 4, and as anticipated from the hypothesis generated from the literature results summarized in Figure 2, these tests indicate that increasing salinity will cause certain fines (such as bentonite) to cluster and settle more quickly, whereas other fines such as kaolin, will respond by settling more slowly than in fresh water.

A second process that was observable during the sedimentation tests was the manner in which sedimentation occurred: uniform segregation occurred when the fines all fell together, whereas segregated sedimentation occurred when the fines had different falling velocities either for the individual particles, or for the individual particles relative to particle clusters that also formed in the fluid (Figure 3).

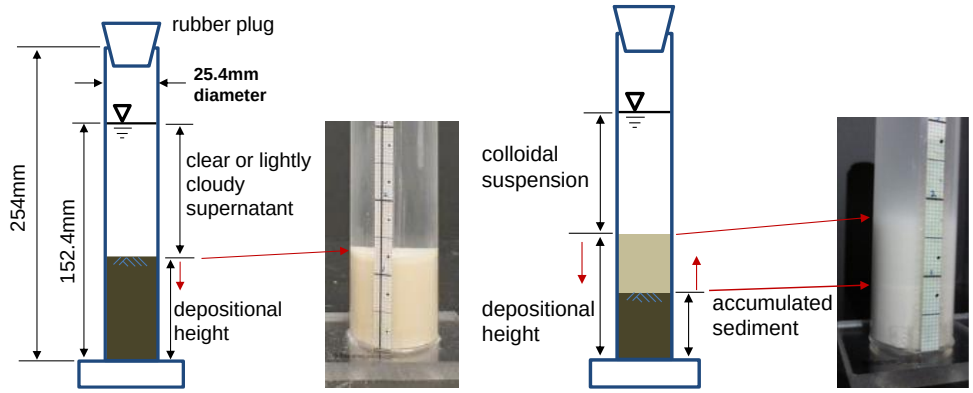

(a) Uniform Sedimentation (b) Segregated Sedimentation

Figure 3. (a) A uniform sedimentation response in which essentially all sediment particles fall together such that a sharp interface is observed at the depositional height between the sediment and overlying clear or lightly cloudy supernatant; (b) a segregated sedimentation response in which the sediment segregates (due to different falling velocities of individually-sized and clustered particles) into a bottom layer containing the largest particles (accumulated sediment), a middle layer extending to the depositional height and containing smaller particles, and an overlying cloudy colloidal suspension containing the finest particles. The directions in which the interfaces move are given by the vertical red arrows.

The sediment fabric has a significant control on the sediment compressibility and permeability. Because the sediment fabric itself is controlled to a large extent by how the fines organize as a test specimen

is being created, trends in the compressibility results (Figure 5) can be anticipated from the sedimentation test results.

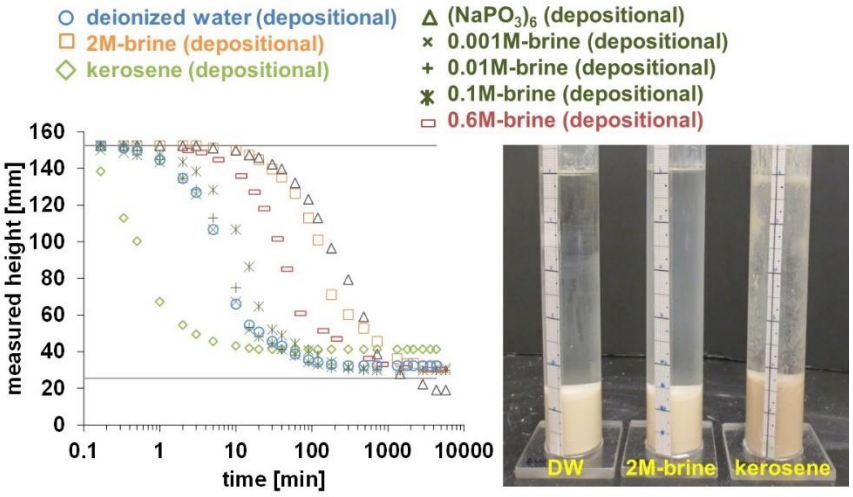

(a) Kaolin

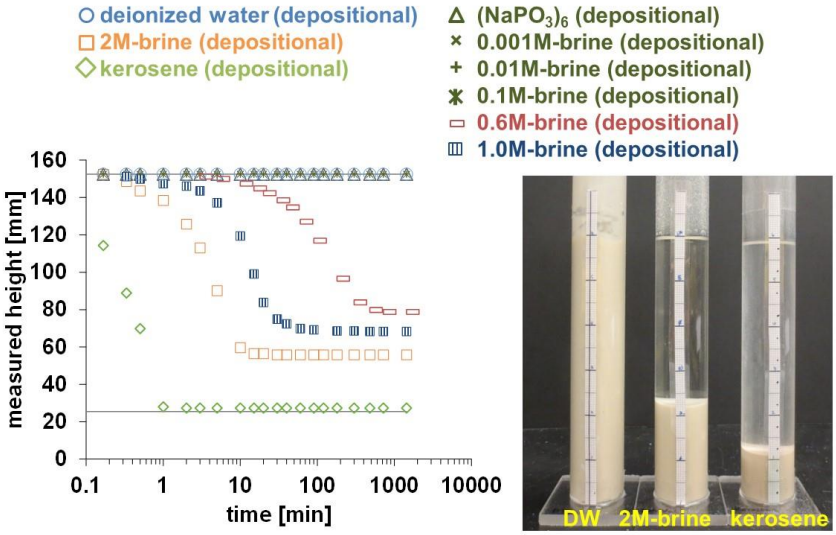

(b) Bentonite

Figure 4. Sedimentation interface heights with time. Horizontal reference lines represent 152.4 mm, the fluid column height; and 25.4 mm, the initial height of each dry, loose-packed specimen. Symbol legends are given in each plot: depositional (open symbols) and accumulated (filled symbols) interface heights refer to the interfaces described in Figure 2. Inset images show examples of each specimen in deionized water, 2M brine and kerosene.

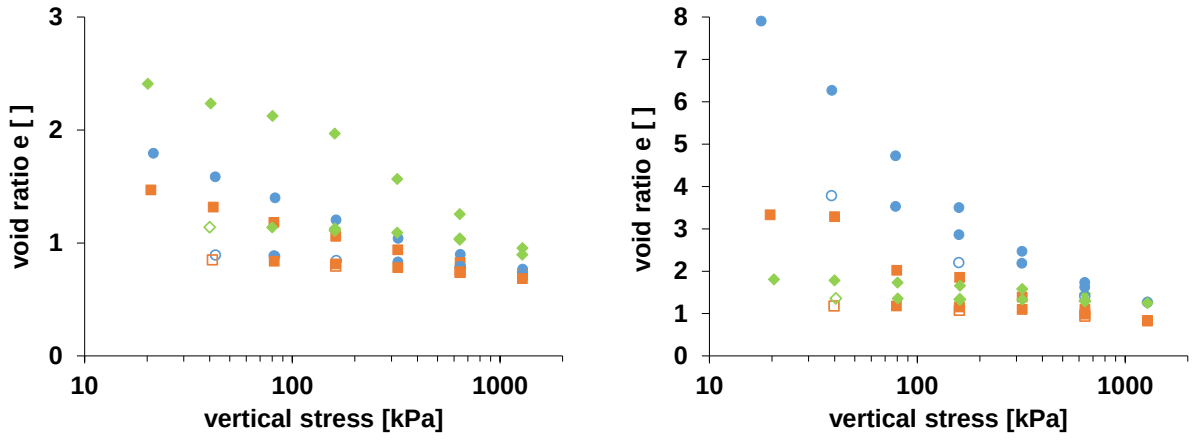

(a) Kaolin (b) Bentonite

Figure 5. Consolidation results in deionized water (circle), 2M brine (square) and kerosene (diamond) for (a) kaolin and (b) bentonite. Solid symbols are loading and reloading steps, and the open symbols are unloading steps. As anticipated from Figures 2 and 4, the initial void ratio is higher for both types of fines in fresh water than in brine, with the difference being much more pronounced in bentonite. This is expected from the large difference in final sedimentation height for bentonite in fresh water and brine relative to kaolin in Figure 4.

The consolidation results are summarized by the compressibility indices given in Table 3 and plotted in Figure 6. The compressibility, being so closely tied to the sediment fabric, varies most significantly for fines that are highly electrically sensitive, and strongly alter their fabric in response to pore-fluid chemistry changes. Whether the fine become more or less compressible as the salinity decreases during pore-water freshening depends on the type of tines. In contrast to the kaolin and bentonite shown in Figure 5, silica silt and diatoms become slightly less compressible as the pore water freshens. For recompression, there is very little dependence on electrical sensitivity because of the tested fines, only bentonite has the capacity to swell and recover a portion of the void space lost to the initial compression. It is important to note, however, that this swelling is greatly enhanced as the pore-water freshens. The results of this study indicate the importance of establishing the mineralogy for a field site of interest as a first step toward estimating how fines in the system will respond to pore water chemistry changes.

Table 3. Compression and recompression indices of endmember sediments.

No.	sediments	compression index C_c			recompression index C_r		
		deionized water	2M brine	kerosene	deionized water	2M brine	kerosene
1	silica silt	0.055	0.094	0.188	0.027	0.03	0.04
2	mica	0.74	0.86	1.174	0.187	0.20	0.25
3	$CaCO_3$	0.138	0.098	0.22	0.025	0.019	0.03
4	diatom	0.39	0.54	1.09	0.106	0.124	0.149
5	kaolin	0.5	0.39	1.12	0.11	0.11	0.16
6	illite	0.39	0.352	0.38	0.06	0.04	0.079
7	bentonite	2.8	1.12	0.385	1.61	0.24	0.075

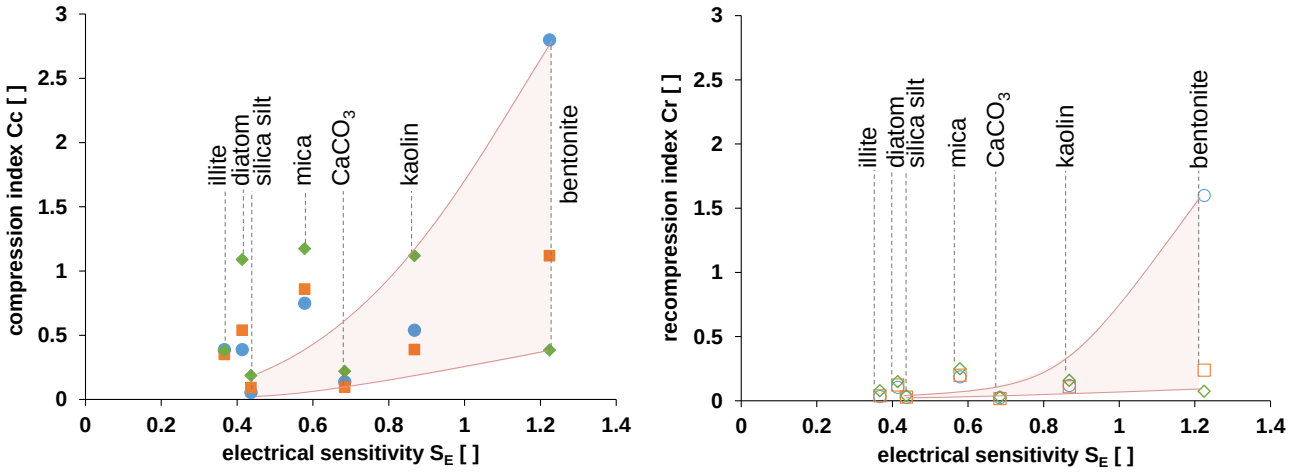

(a) Compression Index, *Cc* (b) Recompression Index, *Cr*

Figure 6. Dependence of the (a) compression (solid symbols) and (b) recompression indices (open symbols) on electrical sensitivity. The shaded area in (a) and (b) represents possible ranges of the compression and recompression index as a function of electrical sensitivity after removing sediments that have unusually high void ratios due to their physical shapes. Symbol shape definitions are the same as in Figure 5.

Primary Task 1 Conclusions: A critical result from Task 1 that impacts Tasks 2 and 3 is the dependence of sediment fabric not only on the type of fines present, but on the pore fluid chemistry. The sediment fabric controls the sediment compressibility, both in terms of what the initial void ratio will be, but also in terms of how the force chains through which the sediment

supports itself are arranged. Figure 7 summarizes how the compressibility depends on the sediment fabric for the cases tested in this task.

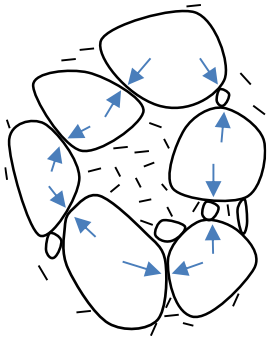

(a) Skeletal force-dominated fabric

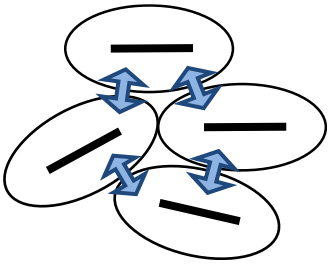

(b) Electrical force-dominated fabric (DDL)

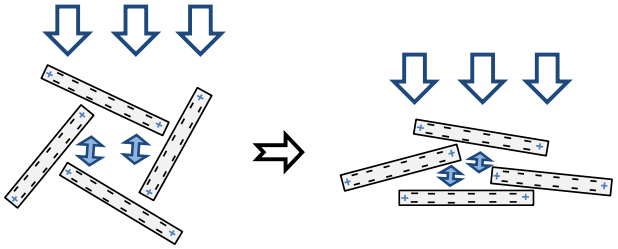

(a) Electrical force-dominated fabric (edge & face)

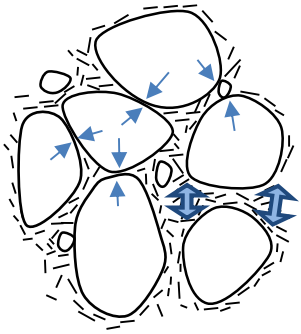

(b) Mixed: skeletal and electrical force

Figure 7. Fabric-based external stress transfer mechanisms. Larger grains are shown as irregular outlined shapes; electrically-sensitive clays are shown as dashes. (a) Skeletal-force dominated fabric, which can form during segregated sedimentation, experiences stress transfer (blue arrows) primarily through contacts between large grains such as silica silt in deionized water. (b) Electrical-force dominated fabric such as the bentonite (dashes) is controlled by DDL thickness (ellipsoids), and thus tends to be relatively compressible. (c) Electrical-force dominated fabric, such as kaolinite, can form high void fabric at low stress and in fresh water, but that fabric is compressible and will collapse under moderate stress. (d) Mixed fabric of skeletal (single-ended arrows) and electrical stress-transfer contacts (double-ended arrows), which can form during homogeneous sedimentation, such as silica silt in 2M-brine, will be more compressible than the purely skeletal force dominated sediment (Hueckel, 1992; Mitchell and Soga, 2005; Santamarina et al., 2001).

Task 2: Fines migration and clogging (2D Micromodels)

Background and Hypothesis: Reservoir permeability is a critical parameter for forecasting the efficiency of extracting methane from gas hydrate-bearing sediment. In a formation produced via depressurization, a pressure gradient drives flow toward the production well. The flow of gas and fresh water from dissociated hydrates has both a physical and a chemical impact on the sediment. This task seeks to distinguish between, and characterize, the effects of both the physical and chemical effects of flow on how fines alter the permeability of host sands.

A physical consequence of flow is to induce sediment particle migration. Even in high-quality gas hydrate reservoir sands, clays or other fines exist in measurable concentrations (Anderson et al., 2014; Egawa et al., 2015; Ripmeester et al., 2005; Winters et al., 2011). Migrating fines can clog pore throats, decreasing permeability in sands.

Clogging can be enhanced by when fines are able to cluster, and as shown in Figure 2, clustering is a function of the type of fines, and the pore-water chemistry. Moreover, pore-water chemistry changes can increase the rate at which fines mobilize (Mohan et al., 1993), increasing the concentration of fines in the fluid flow and increasing the clogging potential.

An additional complexity in producing methane from gas hydrate, the free methane gas from the dissociating gas hydrate forms a gas/water meniscus that can collect and concentrate fines as the meniscus moves. This fines concentration increase is anticipated to accentuate the clogging potential of fines, regardless of the pore-water chemistry or fines type. This project task provides an assessment of the clogging potential of fines via two subtasks:

Subtask 2.1: Clogging potential of pure fines

The pure fines used in Task 1 were also used in 2D micromodel flow tests to generate "clogging maps." These maps indicate the propensity for fines to clog based on their size (relative to the size of the pore throats), their concentration in the flowing fluid, and the fluid type. These tests were

initially run as single-phase flow tests (one fluid per test, either fresh water or 2M brine), and once that test was complete, a reverse-flow test using carbon dioxide (CO_2) gas allowed images of fines clustering at the meniscus and clogging at pore throats.

Subtask 2.2: Clogging potential of natural sediment

Sediment from two gas hydrate research expeditions, the 2010 UBGH2 expedition offshore eastern Korea and the 2015 NGHP-02 expedition offshore eastern India, were characterized and use in 2D micromodel tests to look at their clogging potential. As with Subtask 2.1, tests were conducted for single-phase flow with either fresh water or 2M brine, then subjected to a moving meniscus with CO_2.

Results and Implications: The results summarized here are now published with additional detail in the *Journal of Marine and Petroleum Geology* paper by Cao et al. (2018). For orientation, the micromodel is shown in Figure 8. Single phase flow is from left to right across the micromodel. Dual-phase flow with the CO_2 meniscus, is from right to left across the micromodel.

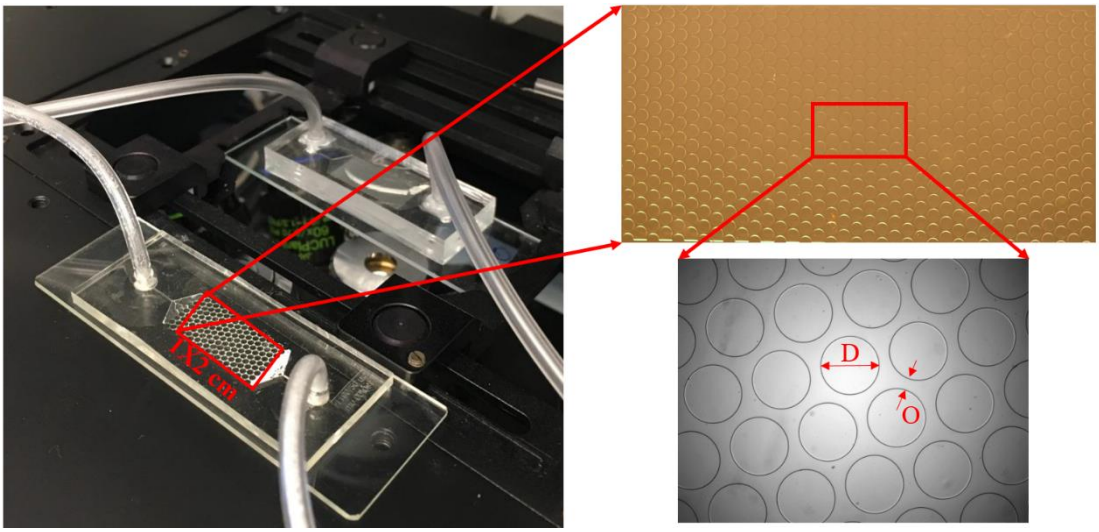

Figure 8. Image of the micromodel with connected fluid and gas flow tubes, and the top (plan view) of the micromodel showing the particle diameter (D) and pore-throat opening (o).

Subtask 2.1: Clogging potential of pure fines

The minimum pore throat width for the micromodels used in this study ranged from 20 to 100 µm, and based on the grain size results from Table 1, individual particles will generally pass through pore throats in that size range. As shown in Figure 9, the individual fines should pipe through the pore throats without clogging.

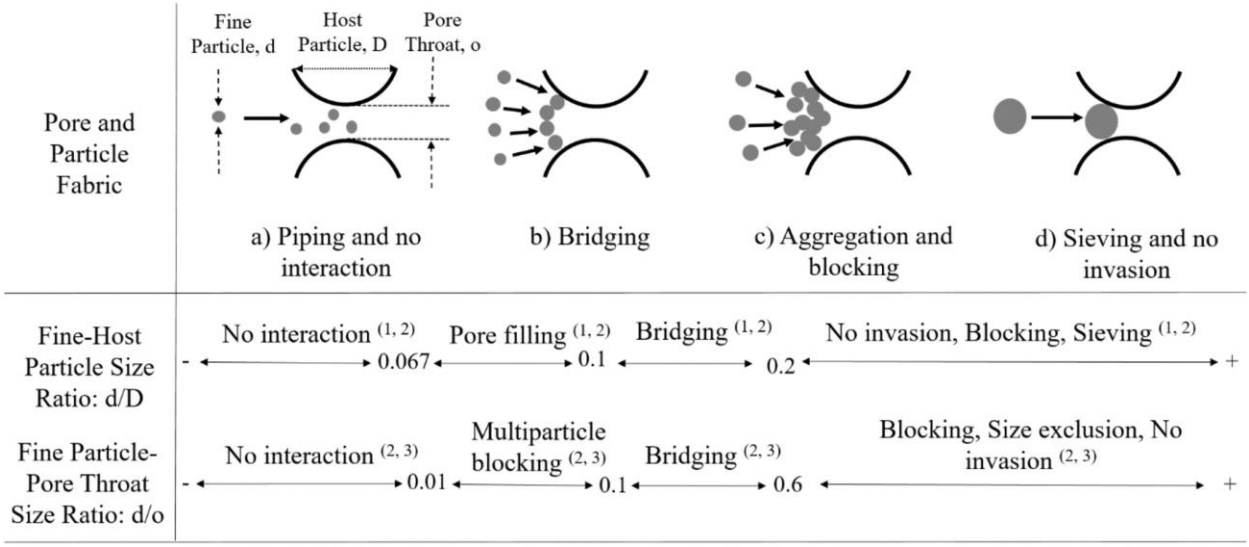

Figure 9. Main mechanisms for fines migrating and clogging at pore throats, classified based on critical size ratios (d/D, d/o). (Host particle diameter (D), fine particle diameter (d), and pore throat width (o)).

Figure 10 shows an example of silica silt passing through a micromodel without clogging when the fluid is pure water, yet clogging when the fluid is 2M brine. As indicated by Figure 2, silica silt particles are better able to cluster in the presence of brine, and by clustering, the silica particles effectively become larger, and can clog pore throats via bridging or aggregation/blocking (Figure 9).

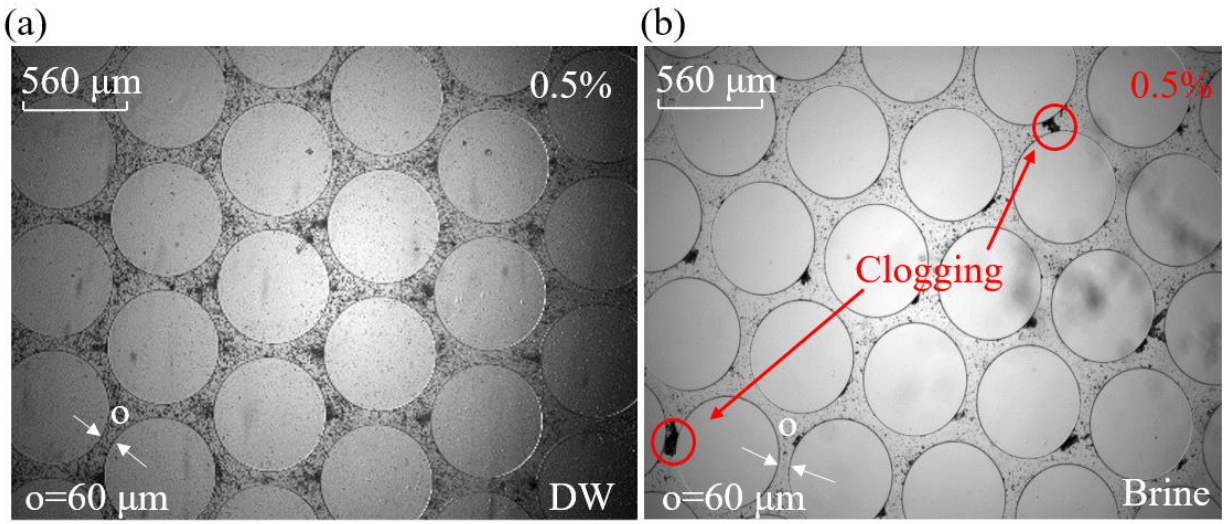

Figure 10. Snapshots of deionized water (DW) and 2M-bine injection with silica silt fines (0.5 % concentration) into the micromodel (o = 60 µm, P = 10 ± 1 kPa). (a) No clogging occurs with 0.5% silica silt for DW, (b) several clogging (red circles) pore throats observed with 0.5 % silica silt for 2M-brine because of the increased clustering ability of the silica silt in brine (e.g. Figure 2).

To capture the dependence of clogging on the fines type, the size ratio between the fines and pore throats, the fines concentration in the fluid and the pore fluid chemistry, clogging maps were made for the pure fines (Figure 11). As can be anticipated from the Task 1 results regarding electrical sensitivity, the electrically-sensitive fines such as bentonite have much larger clogging potential differences as a function of pore fluid than do fines with less sensitivity. Also, as could be anticipated from the Task 1 sedimentation testing and the clustering patters shown in Figure 2, bentonite and kaolin have opposite clogging potential dependencies on pore fluid chemistry. Bentonite, which has a much larger DDL layer in pure water than in brine, effectively pushes particles apart from each other as the pore water freshens, meaning less clustering and hence, less clogging. Kaolin, on the other hand, forms larger clusters, and forms them more rapidly, as the pore water freshens (Figure 2). These larger clusters are better able to bridge and block pores, so clogging becomes more prevalent as pore water freshens in the presence of kaolin. As was the case in Task 1., knowing which fines are present is critical for

understanding whether clogging potential will increase or decrease as pore water freshens.

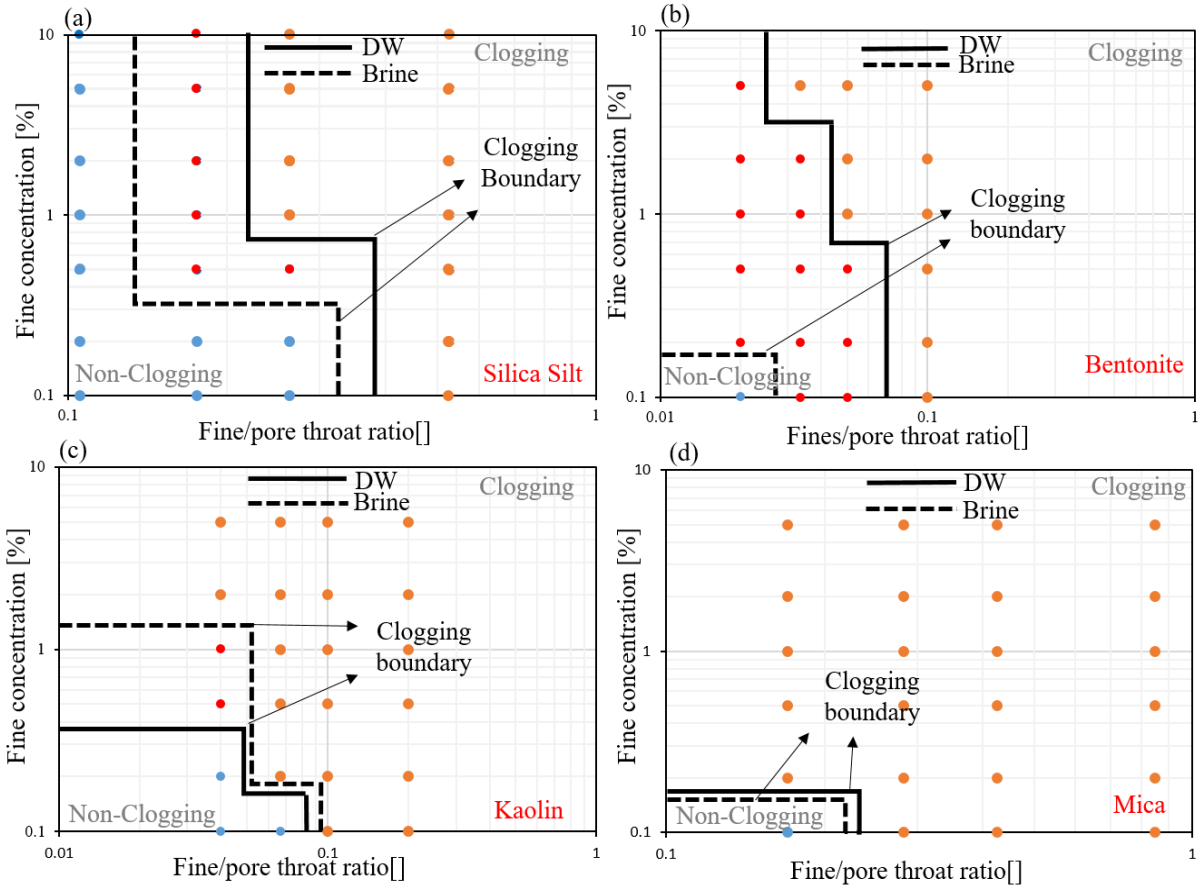

Figure 11. Boundaries between clogging and non-clogging for silica silt, bentonite, kaolin, and mica with fine/pore throat size ratio and fine particle concentration in different pore fluids (DW and 2M brine). Lower left part of each figure represents non-clogging conditions with blue points while the higher right part of each figure represents clogging conditions for both fluids with orange points. Red points between these two extremes represent conditions for which clogging occurs for only one fluid type. (a) Silica silt clogging potential is higher in 2M-brine compared with DW due to positive ions in the 2M-brine attracting silica silt particles into clusters, which are then more prone to clogging, (b) similarly, bentonite particles repel each other in DW and have higher clogging potential in brine due to positive ions in the fluid allowing particles to cluster. The larger gap between the DW and brine boundaries indicates bentonite's high electrical sensitivity to ionic concentration, (c) kaolin has a lower clogging potential in brine due to the smaller face-to-face clusters that form in brines relative to the large edge-to-face clusters that form in DW, (d) Mica, which is a platy particle that clusters similarly to kaolin, also has a lower clogging potential in brine compared to DW.

Diatoms are a special case within this study. Though diatoms are not strongly electrically sensitive, intact diatoms can be over 100 µm in diameter, meaning single diatoms can jam even at the largest pore throats used in this study (Sieving, Figure 9d) without need of clustering with other diatoms or diatom shards.

The presence of a mobile gas/water interface is anticipated to increase the clogging potential by gathering and concentrating fines. A mobile meniscus can be thought of as a means for dramatically enhancing the clustering of fines, and this focusing of fines is evident in the micromodel tests (Figure 12). The enhancement of clogging by the mobile gas water interface, which is an analog for the methane/pore-water interface that migrates toward the production well when extracting methane from gas hydrate, is strong enough to enhance clogging for every type of fine particle in this study.

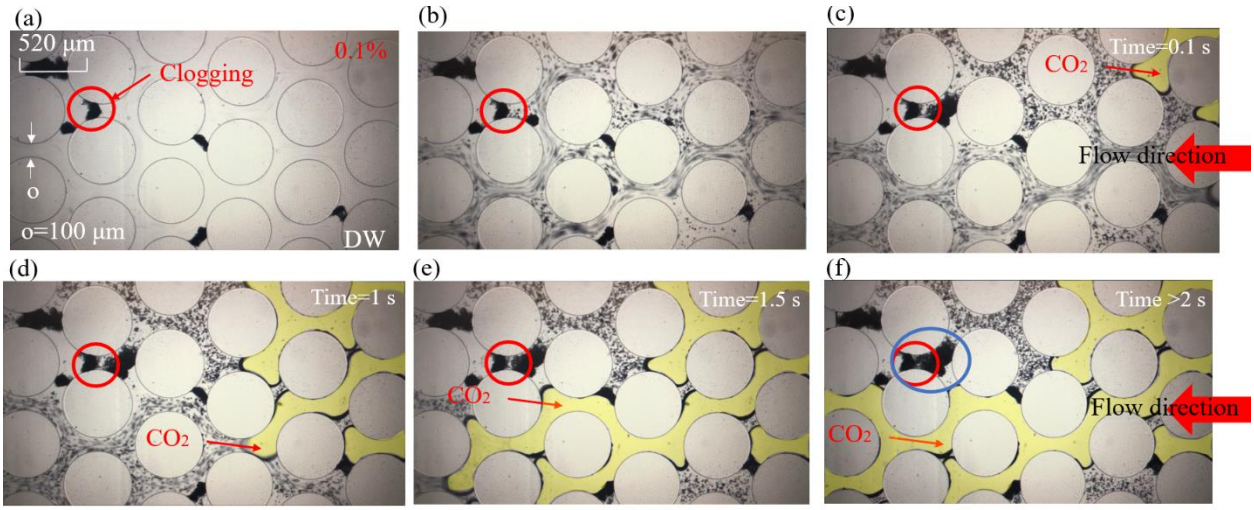

Figure 12. Video snapshots of endmember fine particles (0.1% diatom concentration) migrating in a multiphase (DW/CO_2) flow system (o = 100 µm, P = 10 ± 1 kPa). (a) The final arrangement of fine particles after the single-phase flow test. Red circle indicates the clogging pore throat; (b) fluid and particles migrating ahead of the gas front, which has not yet entered the micromodel. Streaks indicate preferential flow pathways; (c) and (d) CO_2 (yellow region) invading the DW- and fines-saturated micromodel enhances the creation and growth of pore-throat clogs, (e) and (f) more residual water surrounds the clogged pore throat (red circle), and the local fine particle concentration increases in pores (blue circle) as the meniscus pushes fines ahead of the gas flow and appears to strand or isolate pockets of fluid and fines.

Subtask 2.2: Clogging potential of natural sediment

Micromodel tests have been run for two field locations – offshore eastern India (Expedition NGHP-02), and offshore eastern Korea (Expedition UBGH2). The NGHHP-02 results have been published in the *Journal of Marine and Petroleum Science* (Cao et al., 2018), and results are summarized here. The UBGH2 results have been submitted to the *Journal of Marine and Petroleum Science* by Jang et al. (submitted), and are therefore only noted briefly here.

NGHP-02: India's second National Gas Hydrate Program field expedition (NGHP-02) targeted gas hydrate-bearing sands offshore eastern India. For the micromodel study, sediment from the high gas hydrate saturation layers from two sites were tested. Cao et al (2018) contains further details about the geologic settings. In summary, the inferred gas hydrate saturations in both cases exceeded 75%, but the two sites were quite different in their grain sizes and somewhat different in their mineralogies (see Table 4).

Table 4. Sediment characterization for the 2D micromodel material from gas hydrate-bearing sand intervals collected offshore eastern India during NGHP-02.

Site	NGHP-02-09 (Area C)	NGHP-02-16 (Area B)
Core	C8029C-10X-2 W, 9.0-20.0 cm	C8036B-4P-4 WR, 0.0-11.0 cm
Depth (mbsf)	250.975	278.0025
d_{50} (bulk, µm)	754	59
d_{50} (75µm sieve, µm)	32	36
Minerology	**Weight Concentration (%)**	**Weight Concentration (%)**
Quartz	44.1	39.6
Feldspar	43.7	21.9
Mica	5.2	15.7
Carbonate	0	14.3
Chlorite	3.2	4
Illite	0.8	4.6
Kaolinite	1.35	0
Vermiculite	1.5	0

The grain size is a critical element for the 2D micromodels. For NGHP-02-09, an extremely coarse-grained reservoir, the sediment had to be passed through a 75 µm sieve to collect only the fines for 2D micromodel testing. For NGHP-02-16, the median grain size even in the gas hydrate-bearing sand was only 59 µm, so tests could be run on the bulk and sieved sediment. Even using only sediment that had passed the 75 µm sieve, the NGHP-02 sediment had median grain sizes (d_{50}) that exceeded those measured for the pure fines (compare Tables 4 and 1). With larger grain sizes, the NGHP-02 sediment could clog the micromodel pore throat via sieving as well as bridging and blocking (Figure 13).

As shown in Figure 14, the lowest sediment concentration injected into the micromodels in this study was 0.1 wt%, and even this minimum concentration was enough for clogs to form for some of the pure fines such as mica. It is therefore not surprising that the sieved NGHP-02 sediments, being composed of larger particles than the pure fines and containing elevated concentrations of mica, were also susceptible to clogging at low sediment concentrations (< 0.5 wt%).

For single-phase flow, the NGHP-02 sediments showed a very slight reduction in the clogging potential, as indicated by the slight increase in sediment concentration required to initiate clogging (Figure 14). Though this suggests the clogging potential would be reduced during production as the pore water freshened, there are two additional processes that enhance clogging and must be considered. The first is the resuspension process, and fines tend to be more easily resuspended into the pore fluid flow as the pore water freshens (Mohan et al., 1993). Thus, though the clogging occurs at slightly higher sediment concentrations in fresh water, that reduction in clogging will be mitigated because the sediment concentrations are expected to increase as pore water freshens.

The second process to consider is the generation of a gas/water interface during production. As shown for the pure fines, the mobile gas/water interface concentrates fines and enhances clogging. Because the critical clogging concentrations for the NGHP-02 sediments were already at the low end of the concentrations used in this study, the enhanced

clogging expected with the addition of a mobile gas/water interface (advancing CO_2 gas phase) was difficult to distinguish. Though these micromodel studies were keyed to pore throat sizes in the range expected for the NGHP-02 sediments (40-100 μm), larger pore throats or lower sediment concentrations would need to be used to fully capture the clogging enhancement due to the mobile gas/water interface.

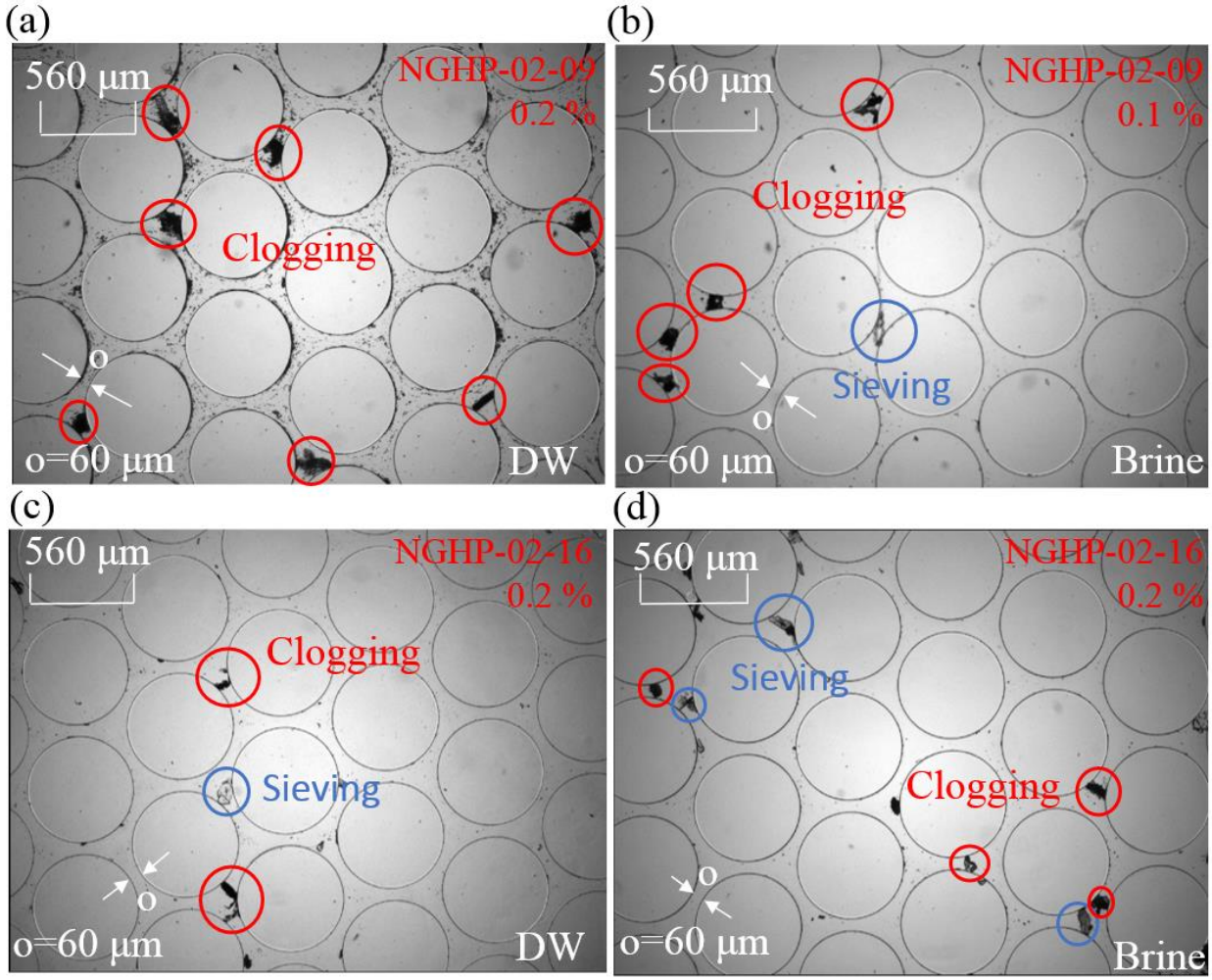

Figure 13. Snapshots of Site NGHP-02-09 and Site NGHP-02-16 sieved fine sediments (d<75 μm) with DW and 2M-brine injection into at the critical clogging concentrations (micromodel pore throat width, o = 60 μm). (a, b) Site NGHP-02-09 fine sediment clogs at 0.2 % concentration in DW, but clogs even lower concentrations (0.1 %) in 2M-brine, (c, d) Site NGHP-02-16 fine sediment clogs at 0.2% concentration in both DW and brine. The overall experimental result shows both Site NGHP-02-09 and Site NGHP-02-16 fines clogging potential does not increase in DW compared with brine. Two clogging mechanisms are observable: red circles indicate pore throat clogging by clusters of fines. Blue circles indicate pore throat clogging caused by individual fine particles (mica) via a sieving mechanism (see also Figure 9).

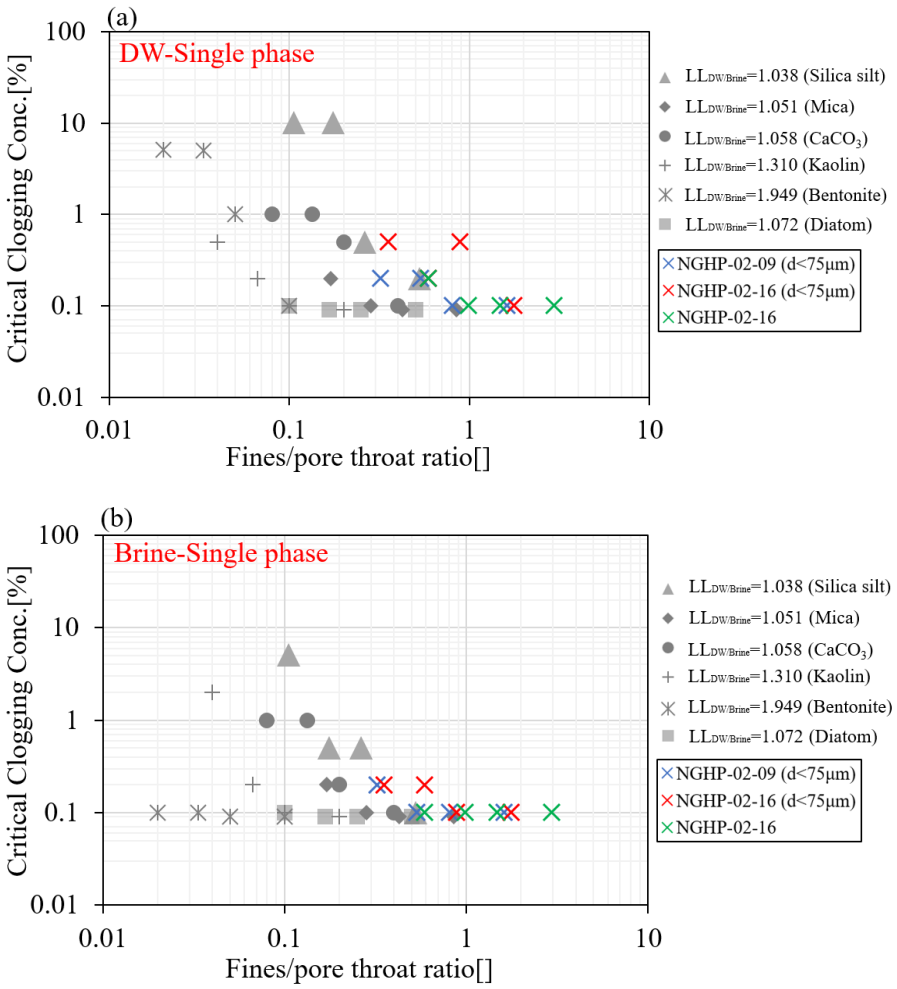

Figure 14. Critical clogging concentration distribution maps for single fluids at different fine-to-pore throat size ratios for pure fines (greyscale symbols) and NGHP-2 fines (colored symbols). (a) Critical fine clogging concentration distribution map for DW, (b) critical fine clogging concentration distribution map for brine. Note the NGHP-02 sediments, which had been sieved through a 75 µm mesh prior to being injected into the micromodel, still contained much larger fines (larger fines/pore throat ratio) than the pure fines. Ratios above 1 indicate a high likelihood of pore-throat clogging via sieving by individual sediment particles (see also Figures 9 and 13).

UBGH2: Korea's second Gas Hydrate field expedition (UBGH2) offshore eastern Korea in the Ulleung Basin, recovered sediment from thin, gas hydrate-bearing intervals of turbidite sands (Ryu et al., 2013). As part of a no-cost extension to the DOE-funded fines project, subsamples from the UBGH2 sediment have been tested in the 2D micromodels. Results from the UBGH2 work is currently under peer review at the *Journal of Marine and Petroleum Geology* in a manuscript by Jang et al. (in review). Full results will be released pending peer review, but key results can be anticipated from the Task 2 results.

The UBGH2 gas hydrate occurrences are in sediment that has been characterized as containing relatively high concentrations of diatoms (Lee et al., 2013). From Figure 14, it can be seen that diatoms have a relatively high clogging potential (clogging at low concentrations), and their prevalence in the UBGH2 sediment is anticipated to yield an overall high clogging potential.

Primary Task 2 Conclusions: Task 2 demonstrates that fines should not all be treated equally in the consideration of clogging during production. The pore water will freshen during production, which causes certain types of fines (such as kaolin) to clog more readily. Other types of fines, such an bentonite, are less likely to clog as the pore water freshens. In natural systems, however, these chemical-based variations in clogging potential are likely to be overshadowed by the increased capacity to mobilize fines as pore water freshens, by the size of the mobile grains, by the presence of a mobile gas/fluid meniscus, and by the geometry of a vertical well bore.

Figure 15 summarizes several clogging processes that can occur during the production of methane from gas hydrate. Conceptually, the clogging processes depicted in Figure 15 all become more effective as either the number of particles or particle size increases. Pore-water freshening should enhance the resuspension of fines, increasing the number of particles in the flowing fluid (Mohan et al., 1993). Moreover,

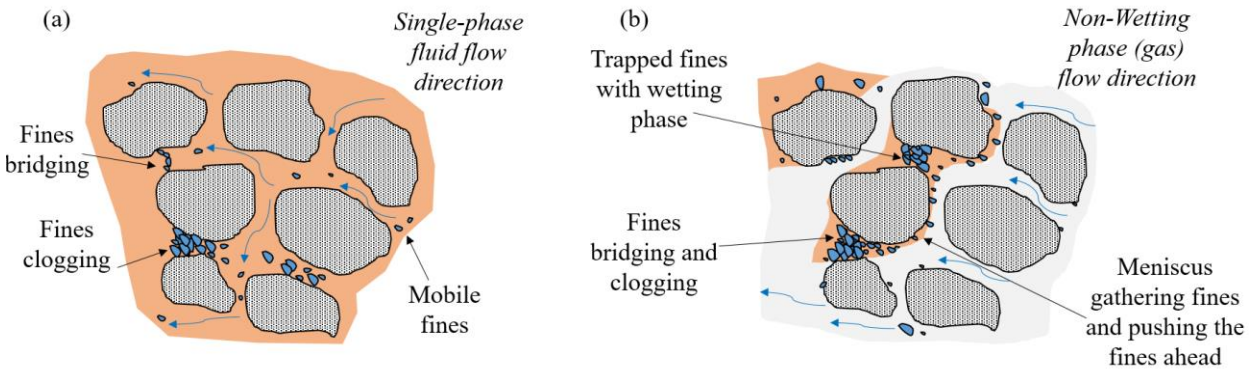

Figure 15. Behavior of fine particle migration and clogging in porous media for both single and two-fluid systems. (a) Single-fluid phase flow promotes fines migration with the flowing fluid (water/brine) unless bridging or blocking occurs at pore throats; (b) when gas invades the wetting phase (water/brine), fines are constrained to move along the gas-liquid interface. That meniscus gathers fines, pushing fines ahead until bridging and clogging happens in pore throats.

when extracting methane from the coarse-grained, gas hydrate-bearing reservoir sediments via depressurization, the fluid flow rates can be large enough to move the coarse sand grains themselves, leading to sand production and the cessation of production activities (Hancock et al., 2019; Li et al., 2016). These flow rates are an order of magnitude larger than what is necessary to mobilize fines (Oyama et al., 2016), so particles of nearly all grain sizes in a given reservoir have the potential to be mobilized. Clogging via bridging, blocking or even sieving will be more likely as the larger particles begin participating in the fluid flow.

The presence of the mobile methane gas/water meniscus will serve to concentrate the resuspended particles, enhancing the clogging beyond what would be anticipated for single-phase fluid flow. Fines concentration will also occur in response to the geometry of a vertical well. As fluid, gas and resuspended particles move radially inward toward the well, they are concentrated as shown in Figure 16, modified from Valdes and Santamarina (2007).

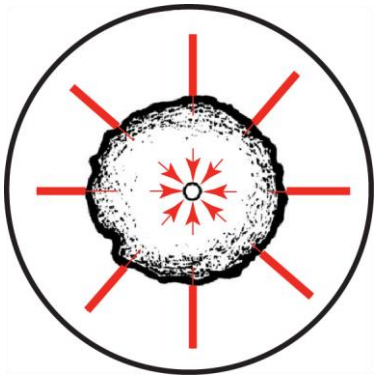

Figure 16. As fluid flows radially inward (solid red lines) toward a well (central black circle), fines migrate inward as well, forming clogging rings (black band around well) that inhibit flow (dotted red arrows). Data image modified from Valdes and Santamarina (2007).

Task 3: Site-specific analysis:

fines impact on compressibility and permeability

Background and Hypothesis: For deepwater gas hydrate occurrences, such as those investigated during the NGHP-02 expedition offshore eastern India, the shape of the gas hydrate stability curve can necessitate large pressure drawdowns to destabilize the gas hydrate and extract the stored methane (Boswell et al., 2018). For the prominent gas hydrate reservoir in Area B of the NGHP-02, for instance, a pressure decrease of ~10 MPa was required to destabilize the gas hydrate, and pressure decreases of nearly 25 MPa were proposed to accelerate the dissociation (Boswell et al., 2018; Myshakin et al., 2018). The 10 or 25 MPA effective stress increases imposed on the gas hydrate reservoir by these pressure drawdowns have significant implications on the evolution of the reservoir. This task looks at the sediment compressibility and permeability, which are linked by the porosity decrease as the sediment compacts due to the imposed effective stress. This Task is split into three Subtasks to evaluate the contribution of fine-grained particles to the compressibility and permeability evolution of the system: Subtask 3.1 provides a characterization of the sediments and sediment grains, Subtask 3.2 assesses sediment compressibility, and Subtask 3.3 focuses on permeability.

Results and Implications: The results summarized here are now published with additional detail in a pair of *Journal of Marine and Petroleum*

Geology papers by Jang et al. (2018). One paper focuses primarily on the gas hydrate reservoir in NGHP-02 Area B, while the second paper assess the seal sediment overlying a prominent gas hydrate reservoir in NGHP-02-Area C.

Subtask 3.1: Characterization of the NGHP-02 sediment

For Area B, the primary sediment analysis was completed on five specimens, one from the overburden seal, one from a sandy gas hydrate reservoir layer, two from finer-grained, essentially gas hydrate-free interbed layers, and one from the underlying sediment. Index property results are given in Table 5, with mineralogy results in Table 6. Both sites listed here, NGHP-02-16 and -23, are at the anticline crest in Area B, where the gas hydrate reservoir is most prominent.

The sediment characterization studies provided several critical insights for the prominent gas hydrate reservoir system targeted in NGHP-02 Area B. In the overburden seal, Logging While Drilling (LWD) results showed an anomalous increase in porosity with depth spanning the interval between 50 mbsf and the top of the gas hydrate-bearing reservoir around 270 mbsf. This porosity trend, which would normally be assumed to decrease with depth due to compaction, could be explained by an increasing concentration with depth of diatoms in the overburden seal, and has been observed elsewhere (Kraemer et al., 2000; Spinelli et al., 2007). In addition to being able to preserve porosity, the presence of diatoms can increase the local permeability relative to diatom-free fine-grained sediment (Bryant and Rack, 1990). This permeability increase, particularly at the interface with the top of the gas hydrate-bearing reservoir, can cause a decrease in the production efficiency of the reservoir (Ajayi et al., 2018; Konno et al., 2018).

Table 5. Index property and specimen characterization for sediment associated with the prominent gas hydrate-bearing reservoir collected offshore eastern India in Area B during NGHP-02. Characterization includes the liquid and plastic limits (*LL* and *PL*) for the largest sediment specimen.

Site No.		NGHP-02-16			NGHP-02-23	
sample ID		633170	640170	634470	585170	590470
sample information		NGHP-02-16B-4P-5, 10.0-22.0cm	NGHP-02-16B-4P-4, 0.0-11.0cm	NGHP-02-16B-7P-2, 110.0-120.0cm	NGHP-02-23B-29X-9, 74.0-86.0cm	NGHP-02-23B-33X-2, 64.0-74.0cm
depth [mbsf]		278.2	278	285.6	262.9	295.2
lithology		sand	sand	pelagic-poor clay	clayey-silt	clay
sediment type		reservoir-fine sand	reservoir-sandy interbed	reservoir-clay interbed	overburden seal	underlying seal
bulk density [kg/m^3]		1470.9	1993.1	2103.2	1501.1	1851.4
grain density [kg/m^3]		2713	2717	2749	2448	2744
porosity [ ]		0.3848	0.354	0.442	0.6924	0.5322
particle size	d_{10} **[mm]**	0.017	0.004	0.0026	0.0021	0.0011
	d_{30} **[mm]**	0.041	0.019	0.011	0.0053	0.0028
	d_{50} **[mm]**	0.0903	0.0356	0.0219	0.0103	0.0053
	d_{60} **[mm]**	0.101	0.048	0.028	0.013	0.007
	d_{90} **[mm]**	0.3067	0.1722	0.0677	0.0478	0.0194
	sand [%]	60.7	32.3	11.3	5.2	0.3
	mud [%]	39.3	67.7	88.7	94.8	99.7
specific surface [m^2/g]		5.8	11.5	35.6	92	69
LL_{DW} **before dilution**						74
***LL* after dilution**	LL_{DW}					61
	LL_{brine}					53
	LL_{ker}					46
S_E						0.31
PL						30

As determined by XRD and by using sedimentation testing methodology described for Task 1, the gas hydrate-bearing units contained primarily silica-type fines, whereas the interbeds and underlying sediment had higher concentrations of smectite (a swelling clay). Silica-type fines, as shown in the Task 2 micromodel studies, tends to clog less readily as the pore-water freshens during production, but this clogging reduction would likely be masked by the elevated fines concentration in the gas hydrate-bearing sands, and the compaction due to the large imposed effective stress. According to a comparison with data compiled by Park and Santamarina (2017), the measured concentration, size distribution, shape

and index properties of the sediment particles in the Area B sands indicate the mechanical and fluid-flow properties of the sands are controlled by fines. The fines control is in spite of the standard d_{50} grain size classification of the sediment as sandy.

Table 6. X-ray-diffraction and smear-slide results for the five Area B specimens described in Table 6, showing the percent (by mass) of the sediment components. Smear slide results provide an independent assessment of the XRD pattern interpretation.

Specimen Environment	reservoir-fine sand (Coarse)	reservoir-sandy interbed (Coarse and fine)	reservoir-clay interbed (Fine)	overburden seal (Fine)	underlying sediment (Fine)
Specimen ID	633170	640170	634470	585170	590470
Depth (mbsf)	278.2	278.0	285.6	262.6	295.2
Material	(%)	(%)	(%)	(%)	(%)
Quartz	47.1	39.6	29.4	13.2	27.8
Feldspar	18.8	21.9	24.6	20.6	16.5
Mica	11.5	15.7	25.4	18.9	32
Carbonate	8.5	14.3	6.3	7.6	1.2
Chlorite	6.2	4	10	10.2	3.59
Illite	3.5	4.6	3.5	29	19.3
Hornblende	4.3	0	1.17	0	0
Sulfides	0	0	0	0.8	0
Smear Slide Comparison	636070	635970	636270	586670	593970
Quartz	89	74	9	3	9.6
Carbonate			30		
Carbonate Mud					25
Carbonate Silt		18			
Clay				30	25
Microfossils				22	
Mudstone			46		
Pyrite				3	
Smear slide designation	Quartz-rich sand	Quartz-rich silt	Silty clay	Diatom-bearing, mudstone-grain-rich, clayey silt	Carbonate-rich clay

As shown in Figure 17, sediments containing both coarse and fine-grained particles have a broad range of potential controls on both its mechanical and flow properties. This sediment characterization, which can be carried out even on the small subsamples available from the cores processed at sea during NGHP-02, provides a means of assessing the compressibility and permeability of the sediment, even when there is not enough sediment available to perform full oedometer or permeameter testing.

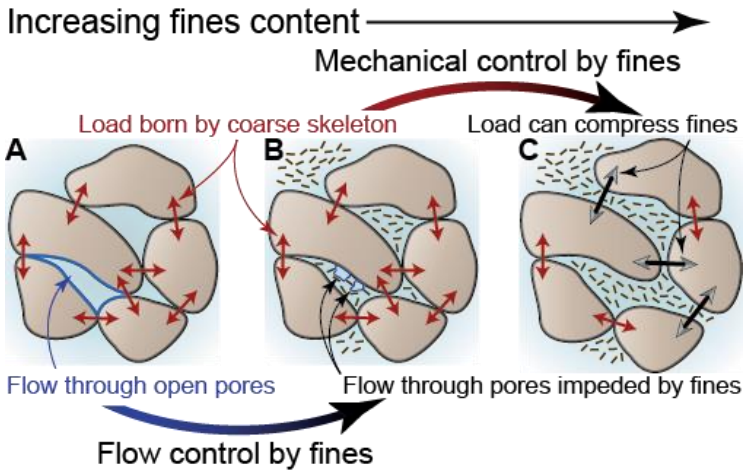

Figure 17. As fines concentration increases, mechanical and flow control over the sediment properties shifts from the coarse to the fine grains. Image modified from Park and Santamarina (2017). The "sands" in Area B are characterized by a balance of particles akin to (c).

Laboratory work by Yoneda et al. (2018) on Area B reservoir sediments demonstrate that these sediments are more compressible than the reservoir sediments from the Nankai Trough, which has dramatic implications for permeability because of the porosity lost as sediment compacts. Given the data from Yoneda et al. (2018), the modeling work for the prominent gas hydrate reservoir in Area B by Myshakin et al. (2018) shows the permeability reduction is far more severe with increasing effective stress than would have been predicted by a standard relationship for coarse-grained sands.

For Area C, a separate study was carried out that made use of sediment recovered from a pressure core taken in the seal sediment interval just above the prominent gas hydrate-bearing reservoir at Site NGHP-02-08. The seal sediment was found to be of low quartz content (10 %), high clay content (>50 %) with low organic material content (~5 %) and a median

grain size d_{50} = 12.27 µm. The microfossil content (~5 %) in the seal layer at Site NGHP-02-08 is less than that (~20 %) in the seal layer above Area B's primary gas hydrate reservoir, suggesting the Area C seal could have better sealing characteristics than the overburden in Area B.

Subtask 3.2: NGHP-02 sediment compressibility

For Area B, the subsamples taken from the shipboard working half of the collected cores were not large enough to accomplish a full oedometer compressibility test, however as indicated in Subtask 3.1, correlations with index property results indicates the Area B reservoir sediments will be more compressible than would be anticipated if the sediments were simply assumed to behave like coarse-grained sediment.

In Area C, results of compressibility tests for the overlying seal sediment are given in Table 7. The compressibility indices are low relative to those for the pure fines measured in Task 1, but this is to be expected given the in situ environmental conditions being tested in this study. The specimens were recovered from nearly 250 mbsf, and had experienced ~2 MPa of vertical stress in situ. At these conditions, the sediment had compacted significantly already, and the remaining in situ void ratio at ~2 MPa vertical stress was only ~0.7 (Figure 18), rather than being 1.5 or greater as was the case for the pure fines (Figure 5).

Table 7. Subsections of pressure core NGHP-02-8B-30P and experimental results from the effective stress cell (ESC) and direct shear cell (DSC). [a] Indicates measurements made after dissociation. [a] Indicates calculation based on Terzaghi's consolidation theory.

Subsection No.		1	2	4	6
Subsection depth [mbsf]		247.63-247.8	247.56-247.63	247.45-247.51	247.12-247.28
measurement chamber		DSC	ESC	ESC	DSC
consolidation indices	C_c	0.289	0.328 0.224[a]	n/a	0.262
	C_s	0.023	0.062 0.028[a]	n/a	0.003
	C_r	n/a	0.081[a]	n/a	n/a
vertical permeability	at 2 MPa	n/a	1.20×10^{-17} m^2 (0.012 mD)	1.22×10^{-17} m^2 (0.012 mD)	5.09×10^{-17} m^2 (0.052 mD)[b]
	at 6 MPa		4.64×10^{-18} m^2 (0.005 mD)	n/a	

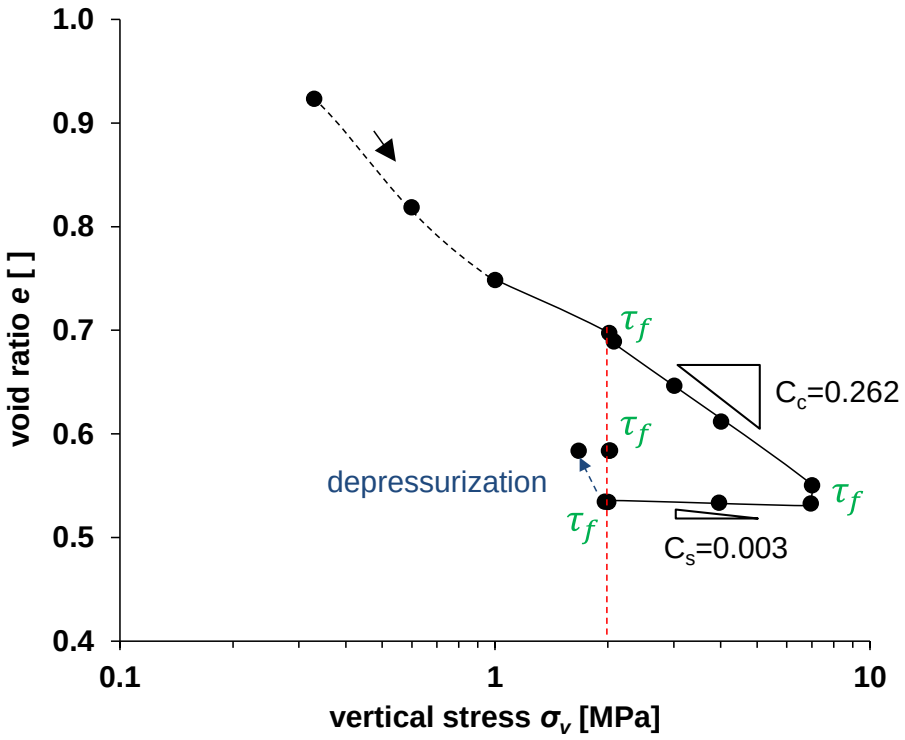

Figure 18. Consolidation results for Subsection 6, as measured in the DSC. Dashed red line is the in situ vertical stress. The initial void ratio at the in situ vertical stress is only 0.7, lower than what was used in the Task 1 (e.g. Figure 5) testing. Correspondingly, the compression index is at the low end of what was measured for the pure fines.

Subtask 3.3: NGHP-02 sediment permeability

For Area B, direct permeability measurements on subsamples taken from the shipboard core collection were not possible due to the small sample volumes. As with compressibility, correlations between the index properties and the permeability are valuable to apply in these cases. Table 8 contains permeability bounds based on correlations between permeability and the sediment index properties.

Table 8. Permeability bounds estimated for the NGHP-02 Area B specimens described in Tables 5 and 6. [1)] Bounded by the estimates from Amer and Awad (1974) and Chapuis (2004), using their equations for unconsolidated, coarse-grained soils. [2)] Bounded by the estimates from Carrier (2003) and Ren and Santamarina (2018), using their equations appropriate for fine-grained sediment.

Sample ID	Permeability [mD]
reservoir-fine sand (633170)	1100 – 1400[1)]
reservoir-sandy interbed (640170)	.0079 – 0.025[2)]
reservoir-clay interbed (634470)	0.0036 – 0.0067[2)]
overburden seal (585170)	0.016 – 0.035[2)]
underlying sediment (590470)	0.0041 – 0.0044[2)]

In Area C, permeability measurements could be made directly on the overburden seal sediment using the Effective Stress Cell (Santamarina et al., 2012), and can also be estimated from Terzaghi's consolidation theory using the pore pressure response over time during consolidation. As shown in Table 7, the vertical permeability at the 2 MPa in situ vertical effective stress was 0.012 mD (direct measurement) and 0.052 mD (consolidation theory). Direct measurements of permeability in the overburden seal were also conducted by Dai et al. (2018) and Priest et al. (2018) at the in situ effective stress, obtaining 0.032 and 0.013 mD, respectively. Based on this remarkable agreement between testing methodologies, a consensus result of 0.02 mD was proposed. As indicated in Figure 19, LWD results indicate the seal permeability is lower than the permeability of the underlying reservoir sediment, even with gas hydrate occupying 60 - 80% of the reservoir sediment porosity (Waite et al., 2018). Evidence of the seal sediment porosity being lower than that of the underlying gas hydrate-bearing sediment prompted a review of what should ultimately be considered the "seal" with regard to gas hydrates and the modified Gas Hydrate Petroleum System approach. Currently, the approach assumes the gas hydrate-bearing sediment itself provides

the limiting permeability barrier, but in a manuscript submitted to the journal *Interpretation* (Jang et al., submitted), it is proposed that sampling and testing the overburden sediment as the "seal" is advantageous.

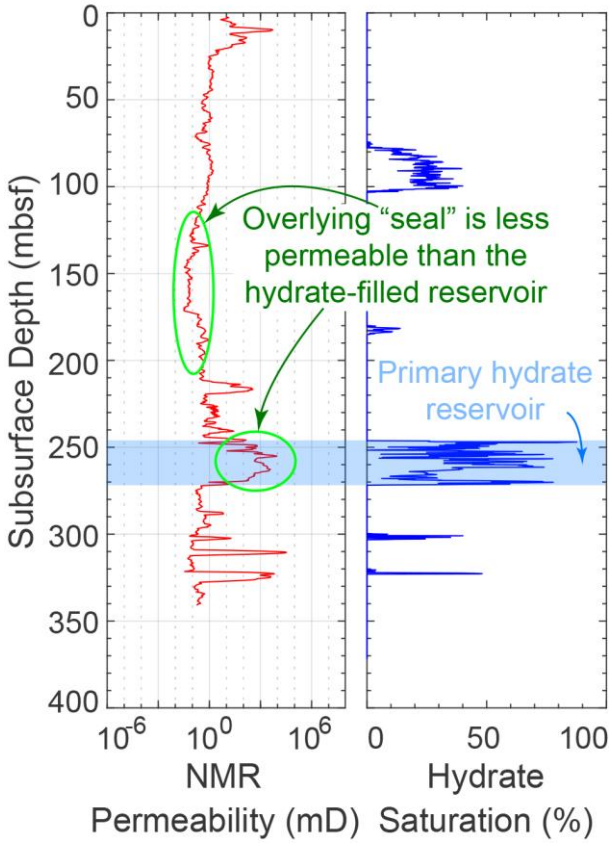

Figure 19. Logging-while drilling data for site NGHP-02-08, showing in situ permeability estimated from the downhole nuclear magnetic resonance tool (NMR), and the Archie-based, pore-space gas hydrate saturation estimate. The primary coarse-grained hydrate reservoir is shaded in blue. Even with the high hydrate saturations hosted in that sediment, the estimated permeability is higher than is estimated for the hydrate-free, fine-grained "seal" sediment overlying the reservoir. Note that hydrate saturation estimates outside of the coarse-grained interval indicate primarily gas hydrate veins in fine-grained sediment, a morphology that tends to cause the Archie approach to overestimate gas hydrate saturation.

Primary Task 3 Conclusions: Task 3 demonstrates the importance of obtaining even small amounts of sediment from the seal, reservoir, and associated sediments. Though there may not be enough material available for running complete oedometer compressibility tests or permeameter assessments of the fluid flow properties, valuable correlations between the index properties, mineralogy and the macroscopic response of the sediment to imposed stresses and flow conditions can be made.

For NGHP-02, a critical outcome is that, given the large effective pressures that will need to be imposed to destabilize the gas hydrate and release the methane for production, compaction will be a primary driver in reducing the sediment porosity, and hence, permeability. As noted by

Boswell et al. (2018), the reservoir production pressure may need to represent a balance between driving rapid dissociation (low drawdown pressure, high effective stress) and preserving the in situ porosity and permeability (moderate drawdown pressure, moderate effective stress).

A second outcome is the recognition that gas hydrate dissociation will likely occur preferentially at the interfaces between gas hydrate-bearing coarse-grained intervals, and fine-grained interbeds (Cohen et al., 2019; Myshakin et al., 2018; Uchida et al., 2018). With fluid flow focused along these interfaces, resuspension of fines from the fine-grained interbeds (or the upper and lower seal interfaces) will be enhanced. Understanding the impact of these fines on the evolution of permeability over the life of a production well is important. Ultimately, characterization of all components of the sediments associated with, and adjacent to, the primary gas hydrate-bearing sediment will be required to fully characterize the reservoir's evolution during production. Though direct geotechnical evaluation of each sediment type in the reservoir/seal system is advisable, assessing the index properties and mineralogy of the fines can provide valuable insights into their behavior when only small amounts of in situ sediment can be recovered.

PRODUCTS

2017

Cao, S.C., Jang, J., Waite, W.F., Jafari, M., Jung, J., A 2D micromodel study of fines migration and clogging behavior in porous media: Implications of fines on methane extraction from hydrate-bearing sediments [Abstract]. Talk presented at the 2017 Fall American Geophysical Union Conference, New Orleans, LA, December 11-15, 2017.

Jang, J., Cao, S., Waite, W.F., Jung, J., Impact of pore-water freshening on clays and the compressibility of hydrate-bearing reservoirs during production. Conference paper accepted by the 9th International Conference on Gas Hydrates, June 25-30, 2017, Denver, Colorado.

Jang, J., Waite, W.F., Jung, J., Pore-fluid sensitivity of clays and its impacts on gas production from hydrate-bearing sediments [Abstract]. Poster presented at the 9th International Conference on Gas Hydrates, June 25-30, 2017, Denver, Colorado.

2018

(note: NGHP ScienceBase data releases will go live when the NGHP-02 special volume is finalized online)

Cao, S.C., Jang, J., Jung, J., Waite, W.F., Collett, T.S., Kumar, P., 2018. 2D micromodel study of clogging behavior of fine-grained particles associated with gas hydrate production in NGHP-02 gas hydrate reservoir sediments, 2018. *Journal of Marine and Petroleum Geology*. https://doi.org/10.1016/ j.marpetgeo.2018.09.010.

Cao, S.C., Jang, J., Jung, J., Waite, W.F., Collett, T.S., and Kumar, P., 2018b. 2D Micromodel studies of pore-throat clogging by pure fine-grained sediments and natural sediments from NGHP-02, offshore India: *U.S. Geological Survey data release*, https://doi.org/10.5066/P9PZ5M7E.

Jang, J., Cao, S., Boze, L.G., Jung, J., Waite, W.F, 2018. Volume change in fine-grained sediments due to pore water salinity changes: gas hydrate-bearing sediments and pore water freshening during gas hydrate dissociation, presented poster at: Fall American Geophysical Conference, December 9-14, 2018, Washington D.C.

Jang, J., Cao, S., Stern, L.A., Jung, J., Waite, W.F., Impact of pore-fluid chemistry on fine-grained sediment fabric and compressibility, 2018. *Journal of Geophysical Research, Solid Earth*: Solid Earth, 123, 5495–5514. https://doi.org/10.1029/ 2018JB015872.

Jang, J., Cao, S. C., Stern, L. A., Waite, W. F., and Jung, J., 2018. Effect of pore fluid chemistry on the sedimentation and compression behavior of pure, endmember

fines: *U.S Geological Survey Data Release*, https://doi.org/10.5066/F77M076K.

Jang, J., Dai, S., Yoneda, J., Waite, W.F., Stern, L.A., Boze, L.-G., Collett, T.S., Kumar, P., 2018. Pressure core analysis of geomechanical and fluid flow properties of seals associated with gas hydrate-bearing reservoirs in the Krishna-Godavari Basin, offshore India, *Journal of Marine and Petroleum Geology*. https://doi.org/10.1016/j.marpetgeo.2018.08.015.

Jang, J., Dai, S., Yoneda, J., Waite, F. W., Collett, T. S. and Kumar, P. (2018-b). Pressure Core Characterization Tool Measurements of Compressibility, Permeability, and Shear Strength of Fine-Grained Sediment Collected from Area C, Krishna-Godavari Basin, during India's National Gas Hydrate Program Expedition NGHP-02: *U. S. Geological Survey data release*, https://doi.org/10.5066/P91XJ7DP

Jang, J., Waite, W.F., Stern, L.A., Collett, T.S., Kumar, P., Impact of fine-grained sediment on the nature and development of a gas hydrate reservoir system investigated during NGHP-02 in the Krishna-Godavari Basin, offshore eastern India (in review), *Journal of Marine and Petroleum Geology*.

Jang, J., Waite, F. W., Stern, L. A., Collett, T. S. and Kumar, P., 2018b. Dependence of sedimentation behavior on pore-fluid chemistry for sediment collected from Area B, Krishna-Godavari Basin during India's National Gas Hydrate Program, NGHP-02: *U. S. Geological Survey data release*, https://doi.org/10.5066/P9FXJ1VX.

Jung, J., Cao, S., Jang, J., Waite, W.F., Lee, J.Y., 2018. Clogging behavior of fines associated with gas hydrate production, from pure fines to NGHP-02 and UBGH-02 reservoir fines, presented talk at: Fall American Geophysical Conference, December 9-14, 2018, Washington D.C.

2019

Jang, J., Waite, W.F., Stern, L.A., Gas hydrate petroleum systems: what constitutes the "seal?". Manuscript submitted to the SEG/AGU collaborative journal *Interpretations*.

Jang, J., Cao, S.C., Stern, L.A., Waite, W.F., Jung, J., Lee, J.Y., Potential freshening impacts on fines migration and pore-throat clogging during gas hydrate production: 2-D micromodel study with diatomaceous UBGH2 sediments. Manuscript submitted to the *Journal of Marine and Petroleum Geology*.

Additional References Used

Ajayi, T., Anderson, B.J., Seol, Y., Boswell, R., Myshakin, E.M., 2018. Key aspects of numerical analysis of gas hydrate reservoir performance: Alaska North Slope Prudhoe Bay Unit "L-Pad" hydrate accumulation. Journal of Natural Gas Science and Engineering 51, 37-43. https://doi.org/10.1016/j.jngse.2017.12.026

Amer, A.M., Awad, A.A., 1974. Permeability of cohesionless soils. Journal of the Geotechnical Engineering Division 100, 1309-1316

Anderson, B., Boswell, R., Collett, T.S., Farrell, H., Ohtsuki, S., White, M., Zyrianova, M., 2014. Review of the findings of the Ignik Sikumi CO2-CH4 gas hydrate exchange field trial, Proceedings of the 8th International Conference on Gas Hydrates, Beijing, China, July 28 - Aug.1, 2014.

Boswell, R., Myshakin, E., Moridis, G., Konno, Y., Collett, T.S., Reagan, M., Ajayi, T., Seol, Y., 2018. India National Gas Hydrate Program Expedition 02 summary of scientific results: Numerical simulation of reservoir response to depressurization. Marine and Petroleum Geology, https://doi.org/10.1016/j.marpetgeo.2018.1009.1026. https://doi.org/10.1016/j.marpetgeo.2018.09.026

Bryant, W.R., Rack, F.R., 1990. Consolidation characteristics of Weddell Sea sediments: Results of ODP Leg 113, in: Barker, P.F., Kennett, J.P. (Eds.), Proceedings of the Ocean Drilling Program, Scientific Results, College Station, TX, pp. 211-223.

Carrier, W.D., 2003. Goodbye, Hazen; Hello, Kozeny-Carmen. Journal of Geotechnical and Geoenvironmental Engineering 129, 1054-1056. https://www.doi.org/10.1061/(ASCE)1090-0241(2003)129:11(1054)

Chapuis, R.P., 2004. Predicting the saturated hydraulic conductivity of sand and gravel using effective diameter and void ratio. Canadian Geotechnical Journal 41, 787-795. https://www.doi.org/10.1139/t04-022

Cohen, E., Klar, A., Yamamoto, K., 2019. Micromechanical Investigation of Stress Relaxation in Gas Hydrate-Bearing Sediments Due to Sand Production. Energies 12, 2131. https://www.mdpi.com/1996-1073/12/11/2131

Dai, S., Kim, J., Xu, Y., Waite, W.F., Jang, J., Yoneda, J., Collett, T.S., Kumar, P., 2018. Permeability anisotropy and relative permeability in sediments from the National Gas Hydrate Program Expedition 02, offshore India. Marine and Petroleum Geology, https://doi.org/10.1016/j.marpetgeo.2018.1008.1016. https://doi.org/10.1016/j.marpetgeo.2018.08.016

Egawa, K., Nishimura, O., Izumi, S., Fukami, E., Jin, Y., Kida, M., Konno, Y., Yoneda, J., Ito, T., Suzuki, K., Nakatsuka, Y., Nagao, J., 2015. Bulk sediment mineralogy of gas hydrate reservoir at the East Nankai offshore production test site. Marine and Petroleum Geology 66, 379-387

Hancock, S., Boswell, R., Collett, T., 2019. Development of deepwater natural gas hydrates, Offshore Technology Conference, Houston, Texas, May 6-9, Paper OTC-29374-MS.

Hueckel, T.A., 1992. Water–mineral interaction in hygromechanics of clays exposed to environmental loads: a mixture-theory approach. Canadian Geotechnical Journal 29, 1071-1086. https://www.doi.org/10.1139/t92-124

Konno, Y., Kato, A., Yoneda, J., Oshima, M., Kida, M., Jin, Y., Nagao, J., Tenma, N., 2018. Numerical analysis of gas production potential from a gas-hydrate reservoir at Site NGHP-02-16, the Krishna–Godavari Basin, offshore India–Feasibility of depressurization method for ultra-deepwater environment. Marine and Petroleum Geology, https://doi.org/10.1016/j.marpetgeo.2018.1008.1001. https://doi.org/10.1016/j.marpetgeo.2018.08.001

Kraemer, L.M., Owen, R.M., Dickens, G.R., 2000. Lithology of the upper gas hydrate zone, Blake Outer Ridge: a link between diatoms, porosity, and gas hydrate, in: Paull, C.K., Matsumoto, R., Wallace, P.J., Dillon, W.P. (Eds.), Proceedings of the Ocean Drilling Program: Leg 164 Scientific Results, pp. 229-236.

Lee, J.-S., Lee, J.Y., Kim, Y.M., Lee, C., 2013. Stress-dependent and strength properties of gas hydrate-bearing marine sediments from the Ulleung Basin, East Sea, Korea. Marine and Petroleum Geology 47, 66-76. https://doi.org/10.1016/j.marpetgeo.2013.04.006

Li, X.-S., Xu, C.-G., Zhang, Y., Ruan, X.-K., Li, G., Wang, Y., 2016. Investigation into gas production from natural gas hydrate: A review. Appl Energ 172, 286-322, https://doi.org/210.1016/j.apenergy.2016.1003.1101. https://doi.org/10.1016/j.apenergy.2016.03.101

McBride, M.B., Baveye, P., 2002. Diffuse double-layer models, long-range forces, and ordering in clay colloids. Soil Science Society of America Journal 66, 1207-1217. https://www.doi.org/10.2136/sssaj2002.1207

Mitchell, J.K., Soga, K., 2005. Fundamentals of soil behavior. John Wiley and Sons, New York.

Mohan, K.K., Ravimadhav, N.V., Reed, M.G., Fogler, H.S., 1993. Water sensitivity of sandstones containing swelling and non-swelling clays. Colloids and Surfaces A: Physicochemical and Engineering Aspects 73, 237-254

Myshakin, E.M., Seol, Y., Lin, J.S., Uchida, S., Collett, T.S., Boswell, R., 2018. Numerical simulations of depressurization-induced gas production from an interbedded turbidite gas-hydrate-bearing sedimentary section in the offshore of India: Site NGHP-02-16 (Area-B). Marine and Petroleum Geology, https://doi.org/10.1016/j.marpetgeo.2018.10.047

Oyama, H., Abe, S., Yoshida, T., Sato, T., Nagao, J., Tenma, N., Narita, H., 2016. Experimental study of mud erosion at the interface of an artificial sand-mud alternate layer. Journal of Natural Gas Science and Engineering 34, 1106-1114, https://doi.org/1110.1016/j.jngse.2016.1107.1067. 10.1016/j.jngse.2016.07.067

Park, J., Santamarina, J.C., 2017. Revised Soil Classification System for Coarse-Fine Mixtures. Journal of Geotechnical and Geoenvironmental Engineering 143. https://doi.org/10.1061/(ASCE)GT.1943-5606.0001705

Priest, J.A., Hayley, J.L., Smith, W.E., Schultheiss, P., Roberts, J., 2018. PCATS triaxial testing: Geomechanical properties of sediments from pressure cores recovered from the Bay of Bengal during expedition NGHP-02. Marine and Petroleum Geology. https://doi.org/10.1016/j.marpetgeo.2018.07.005

Ren, X.W., Santamarina, J.C., 2018. The hydraulic conductivity of sediments: A pore size perspective. Eng Geol 233, 48-54. https://doi.org/10.1016/j.enggeo.2017.11.022

Ripmeester, J.A., Lu, H., Moudrakouvski, I.L., Dutrisac, R., Wilson, L.D., Wright, F., Dallimore, S.R., 2005. Structure and composition of gas hydrate in sediment recovered from the JAPEX/JNOC/GSC et al. Mallik 5L-38 gas hydrate production research well, determined by X-ray diffraction and Raman and solid-state nuclear magnetic resonance spectroscopy, in: Dallimore, S.R., Collett, T.S. (Eds.), Scientific Results From The Mallik 2002 Gas Hydrate Production Research Well Program, Mackenzie Delta, Northwest Territories, Canada. Geological Survey of Canada, Bulletin 585, 7p.

Ryu, B.-J., Collett, T.S., Riedel, M., Kim, G.Y., Chun, J.-H., Bahk, J.-J., Lee, J.Y., Kim, J.-H., Yoo, D.-G., 2013. Scientific results of the Second Gas Hydrate Drilling Expedition in the Ulleung Basin (UBGH2). Marine and Petroleum Geology 47, 1-20. https://doi.org/10.1016/j.marpetgeo.2013.07.007

Santamarina, J.C., Dai, S., Jang, J., Terzariol, M., 2012. Pressure core characterization tools for hydrate-bearing sediments. Scientific Drilling 14, 44-48. https://www.doi.org/10.2204/iodp.sd.14.06.2012

Santamarina, J.C., Klein, K.A., Fam, M.A., 2001. Soils and Waves: Particulate materials behavior, chracterization and process monitoring. John Wiley & Sons, Ltd., New York.

Sogami, I., Ise, N., 1984. On the electrostatic interaction in macroionic solutions. The Journal of Chemical Physics 81, 6320-6332. https://www.doi.org/10.1063/1.447541

Spinelli, G.A., Mozley, P.S., Tobin, H.J., Underwood, M.B., Hoffman, N.W., Bellew, G.M., 2007. Diagenesis, sediment strength, and pore collapse in sediment approaching the Nankai Trough subduction zone. GSA Bulletin 119, 377-390. https://www.doi.org/10.1130/b25920.1

Uchida, S., Lin, J.-S., Myshakin, E.M., Seol, Y., Boswell, R., 2018. Numerical simulations of sand migration during gas production in hydrate-bearing sands interbedded with thin mud layers at site NGHP-02-16. Marine and Petroleum Geology. https://doi.org/10.1016/j.marpetgeo.2018.10.046

Valdes, J.R., Santamarina, J.C., 2007. Particle transport in a nonuniform flow field: Retardation and clogging. Applied Physics Letters 90, 244101, https://doi.org/10.1063/1061.2748850

Waite, W.F., Jang, J., Collett, T.S., Kumar, P., 2018. Downhole physical property-based description of a gas hydrate petroleum system in NGHP-02 Area C: A channel, levee, fan complex in the Krishna-Godavari Basin offshore eastern India. Marine and Petroleum Geology, https://doi.org/10.1016/j.marpetgeo.2018.05.021. https://doi.org/10.1016/j.marpetgeo.2018.05.021

Winters, W., Walker, M., Hunter, R., Collett, T., Boswell, R., Rose, K., Waite, W., Torres, M., Patil, S., Dandekar, A., 2011. Physical properties of sediment from the Mount Elbert Gas Hydrate Stratigraphic Test Well, Alaska North Slope. Marine and Petroleum Geology 28, 361-380. https://www.doi.org/10.1016/J.Marpetgeo.2010.01.008

Yoneda, J., Oshima, M., Kida, M., Kato, A., Konno, Y., Jin, Y., Jang, J., Waite, W.F., Kumar, P., Tenma, N., 2018. Permeability variation and anisotropy of gas hydrate-bearing pressure-core sediments recovered from the Krishna–Godavari Basin, offshore India. Marine and Petroleum Geology, https://doi.org/10.1016/j.marpetgeo.2018.1007.1006. https://doi.org/10.1016/j.marpetgeo.2018.07.006

National Energy Technology Laboratory

626 Cochrans Mill Road
P.O. Box 10940
Pittsburgh, PA 15236-0940

3610 Collins Ferry Road
P.O. Box 880
Morgantown, WV 26507-0880

13131 Dairy Ashford Road, Suite 225
Sugar Land, TX 77478

1450 Queen Avenue SW
Albany, OR 97321-2198

Arctic Energy Office
420 L Street, Suite 305
Anchorage, AK 99501

Visit the NETL website at:
www.netl.doe.gov

Customer Service Line:
1-800-553-7681

NATIONAL ENERGY TECHNOLOGY LABORATORY